Electronic Supplementary Material (ESI) for Soft Matter.

Electronic Supplementary Information

Rheology of 3D Printable Ceramic Suspensions: Effects of Non-Adsorbing Polymer on Discontinuous Shear Thickening

Ria D. Corder,[1,2] Yuan-Jung Chen,[1] Pattiya Pibulchinda,[1†] Jeffrey P. Youngblood,[1] Arezoo M. Ardekani,[2] and **Kendra A. Erk[1*]**

[1]School of Materials Engineering, Purdue University, West Lafayette, IN, 47907, USA

[2]School of Mechanical Engineering, Purdue University, West Lafayette, IN, 47907, USA

[†] Current address: Northwestern University, Evanston, IL, 60208, USA.
[*] Corresponding author (email: erk@purdue.edu).

Effects of Low-Energy Ball Milling on Alumina Particles

The effects of low-energy ball milling on the size, morphology, and surface charge of colloidal alumina particles were explored. First, the bulk alumina particles as received from the manufacturer (**Figure S1a**) were compared with alumina particles that had been combined with DARVAN C-N dispersant and DI water and mixed via low-energy ball milling at 30 rpm for four days (**Figure S1b**). The SEM images do not suggest that any drastic changes in particle size or morphology occur as a result of low-energy ball milling, as irregularly-shaped, submicron-sized particles are observed in both cases, with fewer aggregates observed after addition of the dispersant and low-energy ball milling.

Next, a $\phi_{alumina} = 0.550$ suspension was prepared by combining 55.0 vol% alumina, 4.20 vol% dispersant, and 40.8 vol% DI water in a scintillation vial and mixing manually with a spatula for 5 minutes to in an attempt to minimize the shear forces exerted on the particles during mixing. Then, the spatula-stirred suspension was diluted by 10^{-6} with DI water and placed in a bath sonicator for 15 minutes prior to measurement of the particle sizes and zeta potentials. Data from the spatula-stirred suspension was then compared to that from the $\phi_{alumina} = 0.550$ suspension prepared via low-energy ball milling. Prior to dilution, the spatula-stirred suspension appeared to be more viscous than the ball-milled suspension. The particle size data presented in **Figure S1c** and **Table S1** reveal that low-energy ball milling slightly broadens the particle size distribution (**Figure S1c**), but the average size (**Table S1**) is unaffected by the method of mixing. Notably, the particle zeta potential of the spatula-stirred suspension is less negative than that of the ball-milled suspension (**Table S1**). This likely resulted from incomplete distribution of the dispersant prior to dilution and analysis. Overall, these results indicate that low-energy ball milling has a negligible

effect on the size and morphology of the alumina particles but does aid in distribution of the dispersant, which is beneficial for the preparation of homogenous suspensions.

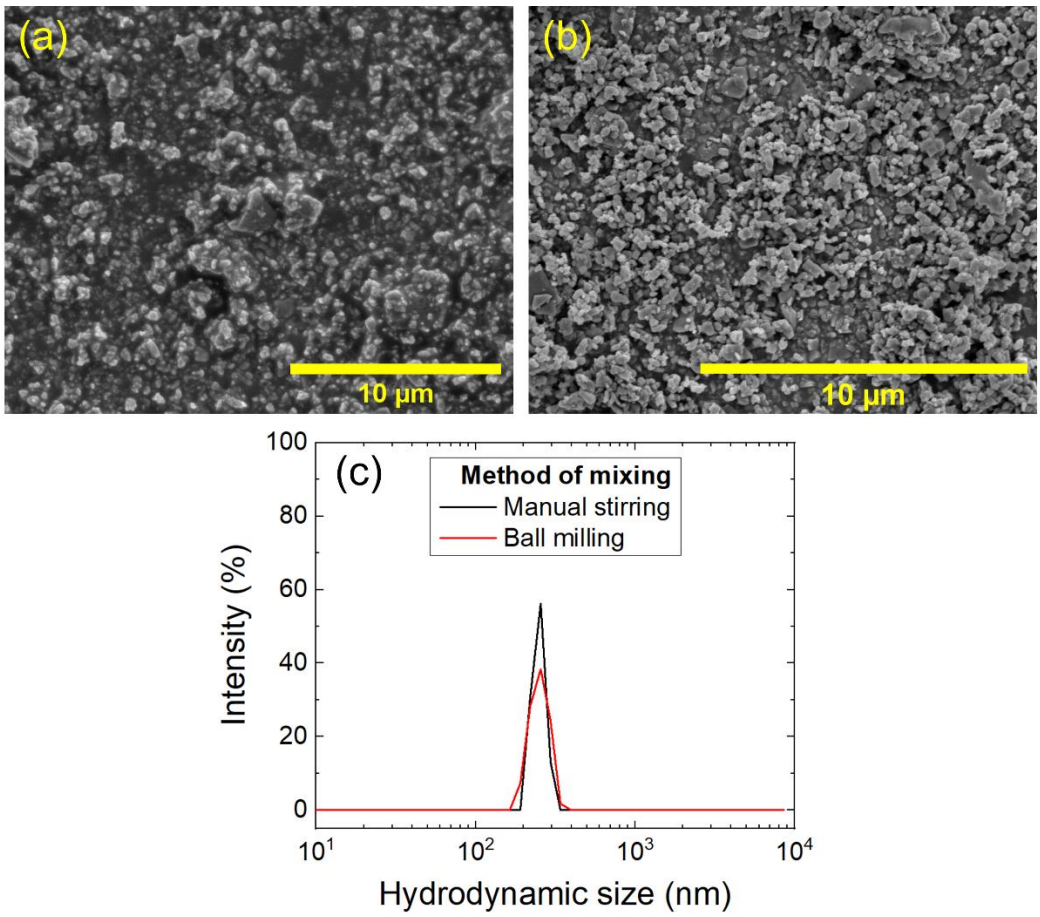

Figure S1. (a-b) SEM images of (a) bulk alumina particles, as received and (b) alumina particles subjected to low-energy ball milling with dispersant in DI water and dried prior to imaging. (c) Particle size distributions of alumina particles from $\phi_{alumina}$ = 0.550 suspensions (both containing 55.0 vol% alumina, 4.20 vol% dispersant, and 40.8 vol% DI water) mixed either by manual stirring with a spatula for 5 minutes or low-energy ball milling for four days.

Table S1. Z-average hydrodynamic sizes and zeta potentials of $\phi_{alumina} = 0.550$ suspensions mixed either by manual stirring with a spatula for 5 minutes or low-energy ball milling at 30 rpm for four days.

Method of mixing	**Z-average size (nm)**	**Zeta potential (mV)**
Stirring via spatula	336 ± 15	-25.0 ± 2.6
Low-energy ball milling	348 ± 15	-47.9 ± 1.1

Data From the Stress Cycling Pre-Shear Conditioning Steps

Data from the pre-shear conditioning steps are provided below for selected suspensions in **Figure S2**. Our stress cycling pre-shear protocol was adapted from the protocol reported by Lee et al.[1] and included two cycles of forward and backward stress ramps from 50-500 Pa (30 s/point, 20 points per decade). Then the forward flow sweep data (reported in full in the manuscript) was collected starting from 50 Pa (30 s/point, 20 points per decade) up to the point at which the rheometer's maximum shear rate limit was reached or the sample yielded or fractured.

The objectives of the pre-shear conditioning protocol were to homogenize the suspension (which could include breaking up aggregates that may have formed within the samples) and to minimize hysteresis between the forward and backward sweeps, particularly in the shear thickening regime. We observe in **Figures S2a-b** that lower viscosity values were obtained during each successive forward step (forward ramps #1 and #2 and the flow sweep), suggesting that the amount of aggregates was reduced[2] by the conditioning protocol. While there is still some hysteresis present between the shear thinning regimes in the backward ramp #2 and flow sweep steps in **Figures S2a-b**, the data in the shear thickening regime is consistent between the two steps. The degree of hysteresis was reduced for the sample with higher viscosity and higher $\phi_{alumina}$ in **Figure S2b** compared to **Figure S2a**. **Figure S2c** shows excellent agreement between the forward ramp #2 and the flow sweep steps in the shear thinning regime and between the backward ramp #2 and flow sweep steps in the shear thickening regime, demonstrating that our protocol was highly beneficial at reducing hysteresis in high-viscosity suspensions containing PVP. In all cases (**Figures S2a-c**), reporting data from only the forward ramp #1 step (e.g. without employing a pre-shear conditioning protocol) would have resulted in inaccurate values for viscosity and τ_{min}.

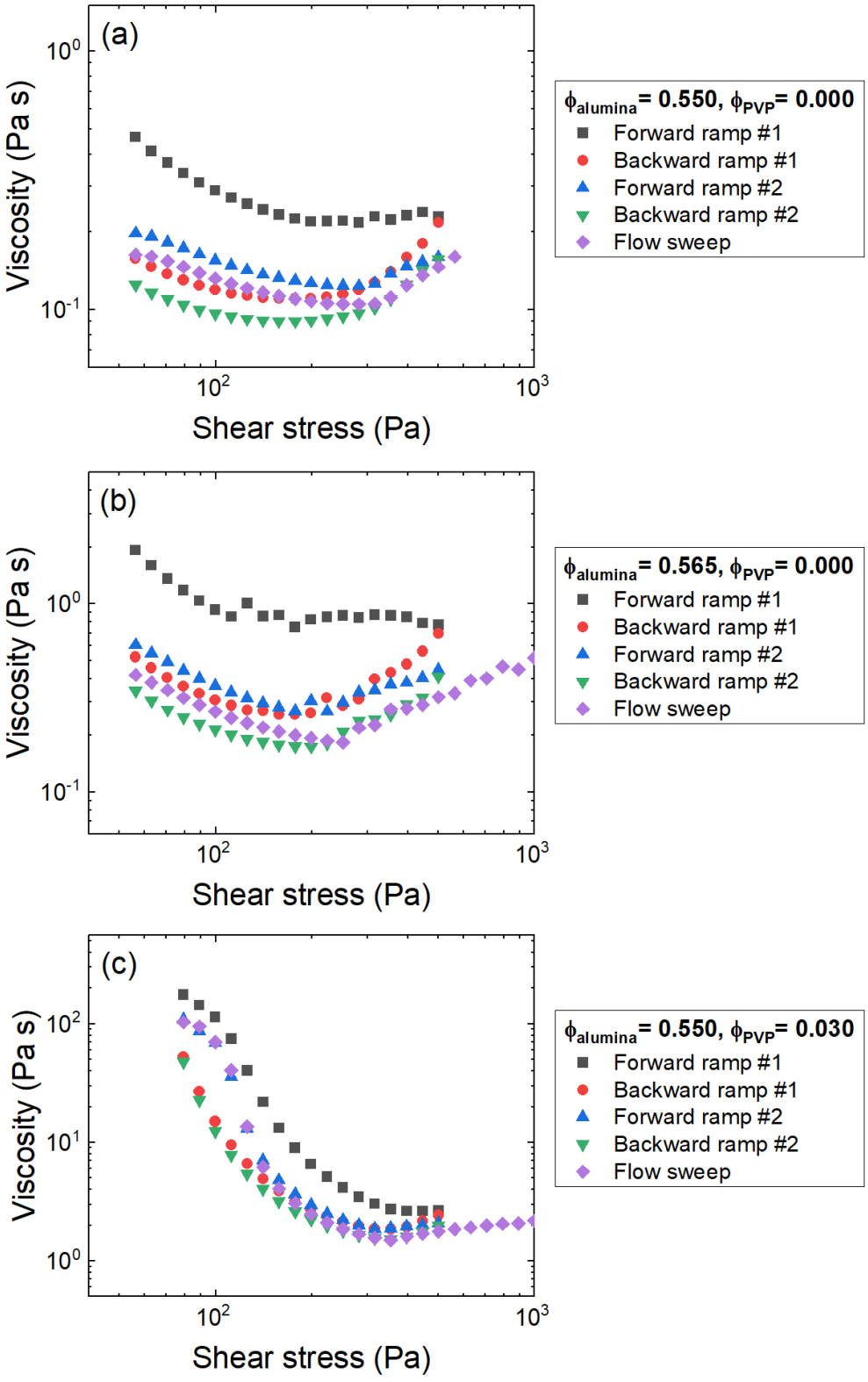

Figure S2. Data from the stress cycling pre-shear conditioning steps for (a) $\phi_{alumina}$ = 0.550, ϕ_{PVP} = 0.000, (b) $\phi_{alumina}$ = 0.565, ϕ_{PVP} = 0.000, and (c) $\phi_{alumina}$ = 0.550, ϕ_{PVP} = 0.030.

Alumina Particle Size Distributions

Representative particle size distributions of alumina suspensions with and without PVP are provided below in **Figure S3**. The data in **Figure S3a** correspond to PVP-free suspensions described in **Table 1**, while the data in **Figure S3b** correspond to PVP-containing suspensions described in **Table 2**. While the distributions in **Figure S3b** of PVP-containing suspensions appear to be slightly more broad than those of the PVP-free suspensions in **Figure S3a**, all distributions are unimodal and centered around ~250 nm.

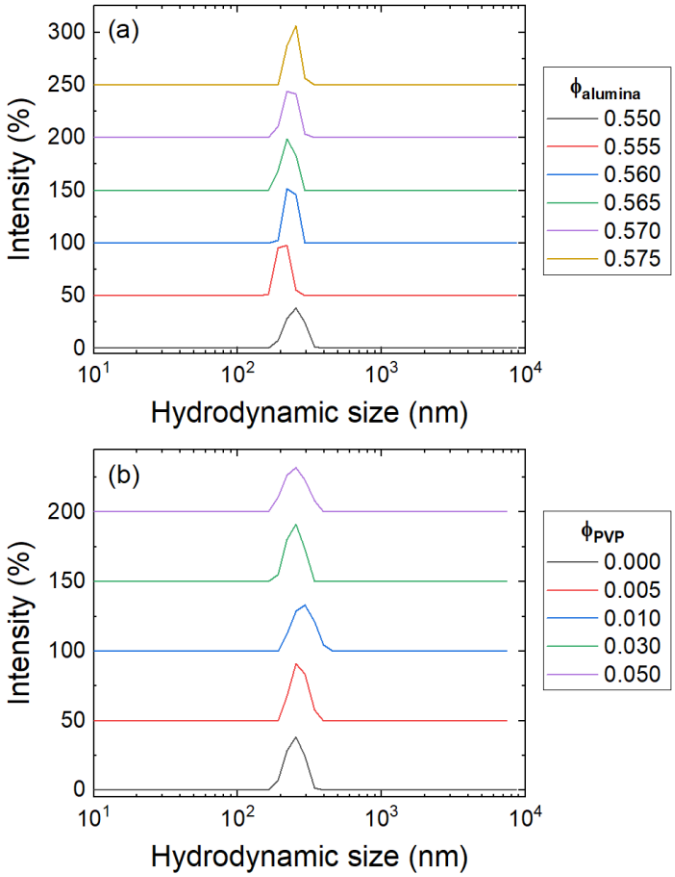

Figure S3. Representative hydrodynamic size distributions of (a) alumina suspensions at varying ϕ and of (b) $\phi_{alumina} = 0.550$ suspensions at varying ϕ_{PVP}.

Generalized Krieger-Dougherty Model Fitting of Minimum and Maximum Relative Viscosities

In our manuscript, we fit the minimum viscosities of each polymer-free alumina suspension prior to shear thickening to a generalized Krieger-Dougherty relation (Eqn. 3), and from that obtained an estimate of the jamming volume fraction. The Wyart-Cates (WC) model[3] is often used to generate state diagrams of systems that exhibit discontinuous shear thickening (DST) and shear-jamming.[4,5] The WC model postulates that two critical volume fractions characterize a system exhibiting DST and shear-jamming, a frictionless jamming volume fraction (ϕ_0), and a frictional jamming volume fraction (ϕ_m). These two critical volume fractions can be estimated using generalized Krieger-Dougherty relations:

$$\eta_{r,min} = \frac{\eta_{min}}{\eta_0} = \left(1 - \frac{\phi}{\phi_0}\right)^{-\beta} \quad \text{Eqn. S1}$$

$$\eta_{r,max} = \frac{\eta_{max}}{\eta_0} = \left(1 - \frac{\phi}{\phi_m}\right)^{-\beta} \quad \text{Eqn. S2}$$

where η_{min} and η_{max} are the lowest (occurring at the onset of shear thickening) and highest (occurring at the conclusion of shear thickening) viscosities, respectively, recorded for each suspension, η_0 is the Newtonian viscosity of the suspending medium, ϕ is the particle volume fraction, and β is a free exponent in each case (usually ≈ 2). Fitting the minimum and maximum viscosity data from **Figure 2a**, as shown in **Figure S4**, results in nearly identical values for ϕ_0 and ϕ_m (0.590 and 0.592, respectively). This suggests that the alumina particles are already in some degree of frictional contact at the minimum viscosity point., Thus, a true value for ϕ_0 cannot be estimated from the existing data. Often, suspensions that exhibit shear-thinning behavior prior to shear-thickening are excluded from fitting to calculate ϕ_0 as the baseline Newtonian viscosity is

obscured.[4–6] However, given that all the suspensions explored herein ($\phi_{alumina}$ = 0.550-0.575) exhibit shear-thinning prior to shear-thickening, we chose to refer in the main manuscript to a general jamming volume fraction, ϕ_J, and not to attempt to fit our data to the WC model.

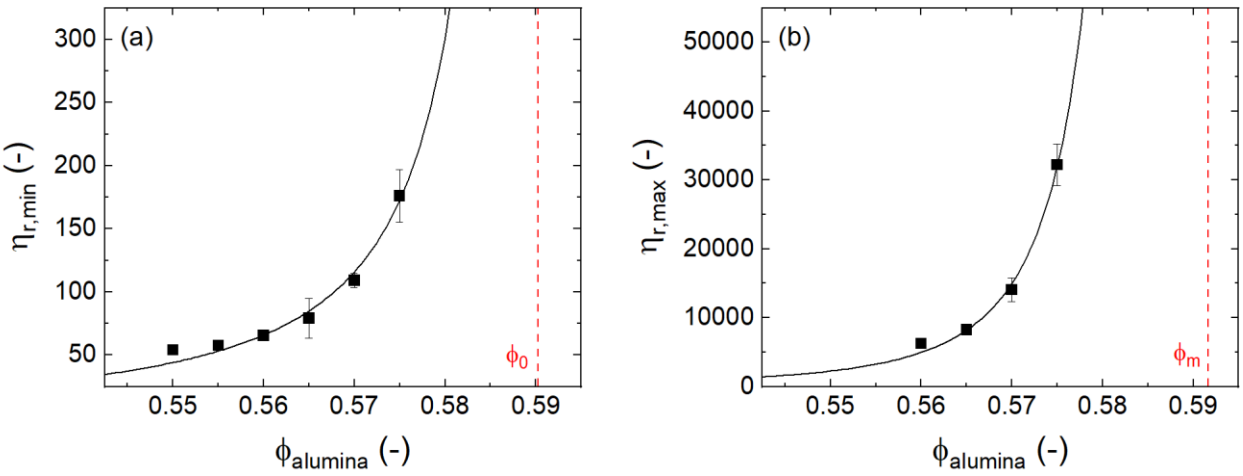

Figure S4. (a) Minimum relative viscosity ($\eta_{r,min}$) vs. $\phi_{alumina}$. The solid black line is the fit to the generalized Krieger-Dougherty model at minimum viscosity (Eqn. S1, β = 1.41, R^2 = 0.938), while the red dashed line denotes the calculated value of ϕ_0 = 0.590. (b) Maximum relative viscosity ($\eta_{r,max}$) vs. $\phi_{alumina}$. The solid black line is the fit to the generalized Krieger-Dougherty model at maximum viscosity (Eqn. S2, β = 2.90, R^2 = 0.975), while the red dashed line denotes the calculated value of ϕ_m = 0.592.

Polymer Solutions Used to Estimate Concentration Ranges for PVP Conformations

Solutions containing DARVAN C-N dispersant, PVP, and DI water were prepared according to the compositions given below in **Table S2**. These solutions matched the composition of the suspending medium for suspensions containing 55 vol% alumina and varying vol% PVP. Each of these solutions exhibited Newtonian flow behavior and their viscosities (provided in **Table S2**) were used to generate **Figure 5** using Eqn. 4.

Table S2. Solution compositions (vol% dispersant, PVP, and water), PVP concentration in the solution ([PVP]), and steady-shear viscosities.

Dispersant (vol%)	PVP (vol%)	DI water (vol%)	[PVP] (g/dL)	Viscosity (mPa s)
9.33	0	90.7	0	1.89 ± 0.24
9.33	0.222	90.4	0.267	2.06 ± 0.16
9.33	0.444	90.2	0.533	2.20 ± 0.10
9.33	0.667	90.0	0.800	2.34 ± 0.20
9.33	0.889	89.8	1.07	2.43 ± 0.20
9.33	1.11	89.6	1.33	2.56 ± 0.10
9.33	1.33	89.3	1.60	2.68 ± 0.14
9.33	1.78	88.9	2.13	2.84 ± 0.13
9.33	2.22	88.4	2.67	2.99 ± 0.28
9.33	4.44	86.2	5.33	4.71 ± 0.24
9.33	6.67	84.0	8.00	7.08 ± 0.24
9.33	8.89	81.8	10.7	10.6 ± 0.1
9.33	11.1	79.6	13.3	15.4 ± 0.3
9.33	13.3	77.3	16.0	20.1 ± 0.2
9.33	17.8	72.9	21.3	42.7 ± 0.3
9.33	22.2	68.4	26.7	82.4 ± 0.1
9.33	26.7	64.0	32.0	164 ± 0.1
9.33	31.1	59.6	37.3	318 ± 0.3

REFERENCES

1 Y.-F. Lee, Y. Luo, T. Bai, S. C. Brown and N. J. Wagner, *Soft Matter*, 2022, **18**, 4325–4337.

2 D. B. Genovese, *Adv Colloid Interface Sci*, 2012, **171–172**, 1–16.

3 M. Wyart and M. E. Cates, *Phys Rev Lett*, 2014, **112**, 098302.

4 N. M. James, H. Xue, M. Goyal and H. M. Jaeger, *Soft Matter*, 2019, **15**, 3649–3654.

5 S. Cao, Y. Wang, H. Pang, J. Zhang, Y. Wu, S. Xuan and X. Gong, *J Rheol*, 2021, **65**, 419–426.

6 S. Dhar, S. Chattopadhyay and S. Majumdar, *Journal of Physics Condensed Matter*, 2020, **32**, 124002.